Journal of Research and Applications in Mechanical Engineering
ISSN: 2229-2152 (Print); 2697-424x (Online)
(2023) Vol. 11, No. 2, Paper No. JRAME-23-11-011
[DOI: 10.14456/jrame.2023.11]

Research Article

Dynamic Mode Decomposition of Flow Around a Circular Cylinder at a Subcritical Reynolds Number

A. Puengrung
K. Septham*
Department of Mechanical Engineering, Faculty of Engineering, King Mongkut's University of Technology Thonburi, Bangkok 10140, Thailand

Received 19 January 2023
Revised 15 March 2023
Accepted 8 May 2023

Abstract:
Flow around a circular cylinder is one of the canonical problems of fluid flows that has been widely studied due to its simple geometries. However, the underlying physics of flow past a circular cylinder is rather complicated. In the present study, flow around a circular cylinder at Re ≈ 3900 is investigated. The unsteady Reynolds-averaged Navier-Stokes (URANS) equations with the k-ω SST turbulent model were employed. The proper orthogonal decomposition (POD), the dynamic mode decomposition (DMD), and the spectral orthogonal decomposition (SPOD) were performed to elucidate the underlying physics of fluid flows in a low-dimensional form. The mean flow structures were extracted through the first POD and DMD mode. The vortex shedding patterns can be detected by the second and third POD mode which are similar to the second mode pair of DMD. SPOD provides three vortex shedding structures from three dominant distinct frequencies. It also indicates that POD requires less modes to reconstruct the mean flow field compared to DMD. It is suggested that the first five most dominant POD modes are sufficient to perform flow reconstruction. The vortex shedding frequencies can be detected via DMD and SPOD.

Keywords: *Proper orthogonal decomposition, Dynamic mode decomposition, Spectral proper orthogonal decomposition, Computational fluid dynamics, Reduced-order models*

1. Introduction

Flow around bluff bodies has been involved in many engineering applications, such as flow past offshore riser pipelines, flow past road vehicles, and flow past buildings. A better understanding of flow physics past these machines and structures is needed to enhance their performance, while minimizing impacts related to flow phenomena. Flow around a circular cylinder is one of the canonical problems of fluid flow that has been widely investigated due to its simple geometries. However, the underlying physics of flow past a circular cylinder is rather complicated consisting of many phenomena such as boundary layer separation, shear layer, wake region, and vortex shedding [1].

Rather than studying the physics through the experimentation, the computational fluid dynamics is utilized for more convenient. Stringer et al. [2] investigated flow past circular cylinder performed by URANS through OpenFOAM. It shows that the URANS developed by Menter [3] is sufficiently accurate compared to the experimental results of Norberg [4]. The flow field data obtained from URANS is large with high dimension. Nevertheless, in the recent years due to the advancement in data-driven methods, the disadvantage of having a tremendous amount of data can

* Corresponding author: K. Septham
E-mail address: kamthon.sep@kmutt.ac.th

be exploited to reduce the dimension of the flow in order to extract significant physics. Data-driven techniques were frequently utilized through the proper orthogonal decomposition (POD) established by Holmes et al. [5] and the dynamic mode decomposition (DMD) introduced by Schmid [6]. Taira et al. [7] applied POD and DMD to flow past circular cylinder at *Re* = 100. They found that the significant structure is the Karman vortex street detected from both POD and DMD at this Reynolds number, where the vortex street is laminar. The regimes of flow past circular cylinder at different Reynolds numbers were illustrated by Lienhard [8] as shown in Fig. 1. However, the data driven techniques have not been used to analyze flow in the subcritical regime. In this work, the flow at *Re* ≈ 3900 is investigated through the POD and DMD to explore the influence of turbulence vortex streets. Furthermore, this work introduces the state-of-the-art data-driven method. The spectral proper orthogonal decomposition (SPOD), recently developed by Sieber et al. [9]. The results obtained from SPOD are compared to those obtained from POD and DMD.

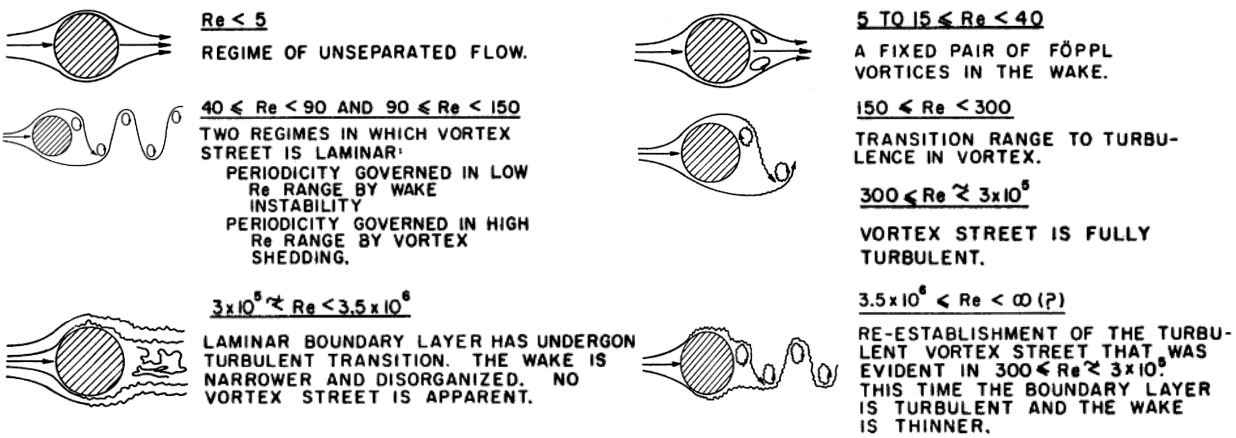

Fig. 1. Regimes of fluid flows around a circular cylinder [8]

2. Methodology

2.1 Unsteady Reynolds-Averaged Navier-Stokes simulations

The Unsteady Reynolds-averaged Navier–Stokes (URANS) equations are utilized to simulate flow around the circular cylinder at *Re* ≈ 3900 through OpenFOAM, which is the open source CFD program in C++ program language. The momentum and continuity equations are presented in Eqs. (1) - (2), respectively.

$$\frac{D\bar{u}_i}{Dt} = \frac{\partial \bar{p}}{\partial x_j} + \nu \frac{\partial^2 \bar{u}_i}{\partial x_j \partial x_j} - \frac{\partial \tau_{ij}}{\partial x_j} \tag{1}$$

$$\frac{\partial \bar{u}_i}{\partial x_i} = 0 \tag{2}$$

where τ_{ij} are the nonlinear Reynolds stress terms. Thus, the Boussinesq hypothesis was introduced to solve the URANS equations by defining the Reynold stress terms in term of the dynamic eddy viscosity (μ_t), which modelled by the $k-\omega$ SST turbulence model.

2.2 Proper Orthogonal Decomposition (POD)

The fundamental concept of POD was to decompose the matrix data set (*Y*) which members are $y_{i,j}$ into the form of a linear combination of orthonormal vectors ($u_{i,m}$). Each element of matrix *Y* can be defined as follows:

$$y_{i,j} = \sum_{m=1}^{N_m} a_{m,j} u_{i,m} \tag{3}$$

where $i \in \{1,2, \dots, N_e\}$, $t \in \{1,2, \dots, N_m\}$ and $a_{m,j}$ are the temporal coefficients. The singular value decomposition (SVD) was connected to POD and used to obtain the POD basis function. The SVD can describe the data set by

$$Y = \psi \Sigma \phi^T \tag{4}$$

where Σ is the elements containing the square root of eigenvalues. The elements in the matrix ψ, Σ and Φ are ψ_i, σ_i and Φ_i respectively. It is noted that ψ and Φ are eigenvectors of YY^T and Y^TY, respectively. Then, equation (5) was transformed into a linear combination form by decomposing the identity matrix to $\psi_i \psi_i^T$.

$$Y = \sum_{i=1}^{d} (\psi_i^T Y_i)\psi_i \tag{5}$$

where d is the rank of Σ. Now, equation (3) is similar to equation (5). So, ψ_i can be defined as POD basis functions or orthonormal vectors. The inner product ($\psi_i Y_i$) represents temporal coefficients. The flow field data have applying in POD by Matlab program.

2.3 Dynamic Mode Decomposition (DMD)

The dynamic mode decomposition began with the transformation of data to the first matrix by gathering the information of the flow in terms of snapshot sequences or each row defined by each time series that has the coordinate of the flow field in the column.

$$X = \begin{bmatrix} \vdots & \vdots & \vdots & \cdots & \vdots \\ x_1 & x_2 & x_3 & \cdots & x_{m-1} \\ \vdots & \vdots & \vdots & \cdots & \vdots \end{bmatrix}, \qquad \acute{X} = \begin{bmatrix} \vdots & \vdots & \vdots & \cdots & \vdots \\ x_2 & x_3 & x_4 & \cdots & x_m \\ \vdots & \vdots & \vdots & \cdots & \vdots \end{bmatrix} \tag{6}$$

where the data with time series $t = x_1, x_2, x_3, \dots, x_m$. The matrix X represents the present flow field. The matrix-free formulation was created to predict the future flow field. The matrix $\acute{X}$ for the future flow field created by converting each time series in the matrix X with a time step (Δt). The data snapshot matrix X and matrix $\acute{X}$ were nonlinear dynamical systems. Now, the relationship of the matrix-free or matrix A can be created by using the optimum linear approximation in equation (7).

$$\acute{X} \approx AX \tag{7}$$

Then, the matrix A can be found by using the Moore-Penrose pseudoinverse to transform matrix X in inverse form of X. After applying SVD to equation (7), the Moore-Penrose pseudoinverse of matrix X can be obtained as follows:

$$A = \acute{X} X^{\dagger} = \acute{X}(V\Sigma^{-1}U^*) \tag{8}$$

The rank of matrix A can be reduced to $r \times r$ by decomposing A in term of U and U^*. The projection of A on the POD modes is defined to be $\tilde{A}$.

$$\tilde{A} = U^* A U = U^* \acute{X} V \Sigma^{-1} \tag{9}$$

Then, eigenvectors W can be obtained by the eigendecomposition of $\tilde{A}$. After finding eigenvectors W, the DMD modes are

$$\Phi = \acute{X} V \Sigma^{-1} W. \tag{10}$$

The algorithm of DMD was write and perform in Matlab program.

2.4 Spectral Proper Orthogonal Decomposition (SPOD)

The key concept of SPOD is to add a time variable from the common space POD. The first step is to partition the $N \times M$ data matrix Q into N_b blocks, whereas each block is of dimension $N \times N_b$.

$$Q = \begin{bmatrix} \overbrace{\vdots \quad \vdots}^{Q^1} & \vdots & \overbrace{\cdots \quad \vdots}^{Q^{Nb-1}} & \vdots \\ q_1 \quad q_2 & q_3 & \cdots \quad q_{(M-1)} & q_M \\ \vdots \quad \underbrace{\vdots}_{Q^2} & \vdots & \cdots \quad \underbrace{\vdots}_{Q^{Nb}} & \vdots \end{bmatrix} \tag{11}$$

Then, the fast Fourier transformation (FFT) was applied into each block of data to convert the flow dynamics from the time domain to the frequency domain. Frequency matrix can be constructed by picking up the same frequency element of each block as shown in equation (12).

$$\widehat{Q}_{f_k} = \sqrt{\Delta t / sN_b} \begin{bmatrix} \vdots & \vdots & \vdots & \cdots & \vdots & \vdots \\ \widehat{q}^1{}_k & \widehat{q}^2{}_k & \widehat{q}^3{}_k & \cdots & \widehat{q}^{N_b-1}{}_k & \widehat{q}^{N_b}{}_k \\ \vdots & \vdots & \vdots & \cdots & \vdots & \vdots \end{bmatrix} \tag{12}$$

where $k = 1, 2, \ldots, N_f$. Then, the calculation of matrix M of frequency k is performed to find eigenvectors (θ_{f_k}) and eigenvalues ($\widetilde{\Lambda}_{f_k}$). The calculation of matrix is presented in equation (13).

$$M_{f_k} = \hat{Q}_{f_k}{}^{*} W \hat{Q}_{f_k} \tag{13}$$

Finally, the SPOD mode of frequency k ($\tilde{\psi}_{f_k}$) can be obtained.

$$\tilde{\psi}_{f_k} = \hat{Q}_{f_k} \theta_{f_k} \widetilde{\Lambda}_{f_k}{}^{-1/2} \tag{14}$$

It is noted that the SPOD mode at each frequency has N_b energy modes.

3. Computation Domain

The dimensions of the computational domain are defined according to the suggestions of Liu [10]. Furthermore, Rajani et al. [11] have complied the domain of numerous researchers of the flow past circular cylinder at $Re \approx 3900$, they defined the length of the cylinder to be πD. The diameter of a circular cylinder is 0.1 m. In the streamwise direction, the distance from the inlet to the cylinder is 1 m and the distance from the cylinder to the outlet is 2.5 m. In the wall-normal direction, the distance from the top wall to the cylinder and the distance from the bottom wall to the cylinder are equal to 0.8 m. The length of the cylinder is 0.314 m along the spanwise direction. The maximum value of y^+ is chosen to be 0.3. The inlet velocity is 1 m/s. To obtain the Reynolds number of 3900, the kinematic viscosity is equal to 2.56×10^{-5} m^2/s. The pressure at the outlet is 0 Pa. Slip wall boundary conditions are defined on the top and bottom walls. Symmetry planes are defined on the side walls. No-slip boundary condition is defined over the cylinder surface. The turbulent energy is equal to 1.5×10^{-4} m^2/ s^2. The specific turbulent dissipate rate is 0.2236 s^{-1}.

4. Results and Discussion

4.1 The Unsteady Reynolds-Averaged Navier-Stokes (URANS)

The results obtained from URANS the $k-\omega$ SST turbulence model using OpenFOAM well agreed with experimental values as shown in Fig. 2 - Fig. 4. Drag coefficient (C_D) and Strouhal number (St) obtained from the simulations are 1.1237 and 0.196, while the experimental values are $C_D = 0.98 \pm 0.05$ and $St = 0.215$.

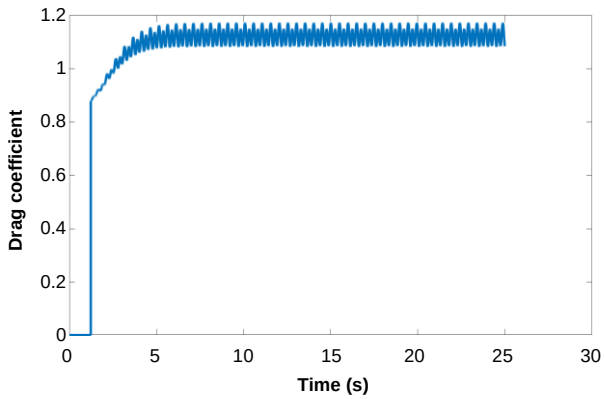

Fig. 2. Drag coefficient vs time

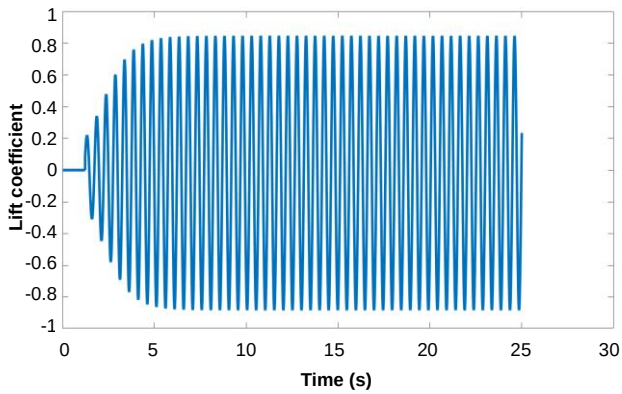

Fig. 3. Lift coefficient vs time

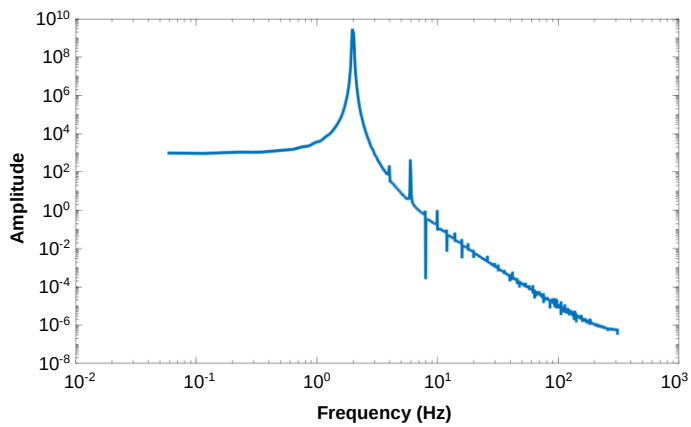

Fig. 4. The frequency spectra of lift coefficient

4.2 Proper Orthogonal decomposition (POD)

Figure 5 presents energy fractions of 340 modes. It reveals that practically most of the energy is contained in the first POD mode. The energy fractions of the second to the tenth most energetic POD modes are illustrated in Fig. 6. Figure 7 shows that as the number of POD modes employed for the flow reconstruction increases, the streamwise velocity of the reconstructed flow field becomes closer to the streamwise velocity obtained from URANS. In the present study, the first five dominant modes can reconstruct the flow field containing 99.97% of the energy of the original flow field. Moreover, the first POD mode represents the spatial structures of the mean flow as shown in Fig. 8. The spatial patterns in the second and third POD modes are large scale *Kármán vortex street*, which are in the state of the rolled-up free shear layer. The top and bottom free shear layers are rolled up to form the vortices at the rear of the cylinder. The fourth and fifth modes represent the smaller scales, though there are additionally relationships between vortices that interact with one another. As can be seen, the vortices on either side are of the center of the rear area are connected. These five modes exhibit perturbation with no decay over time.

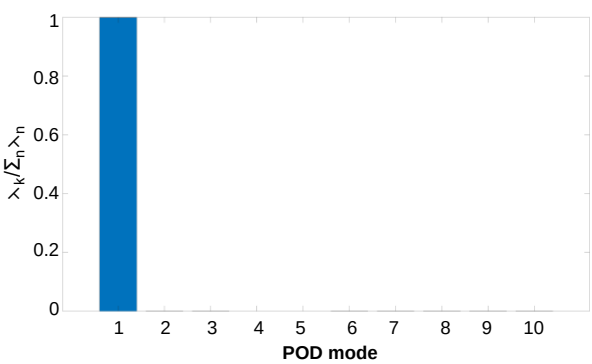

Fig. 5. Energy fractions of the first ten POD modes.

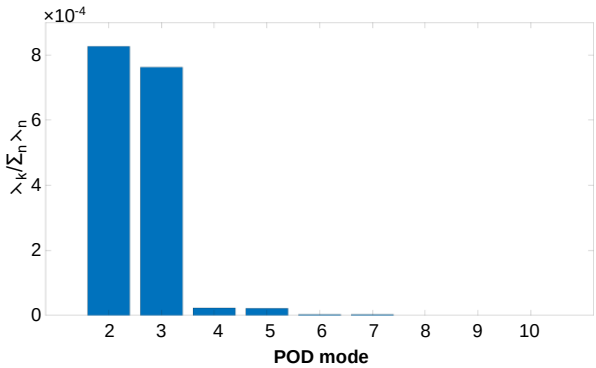

Fig. 6. Energy fractions of the 2nd to the 10th POD modes.

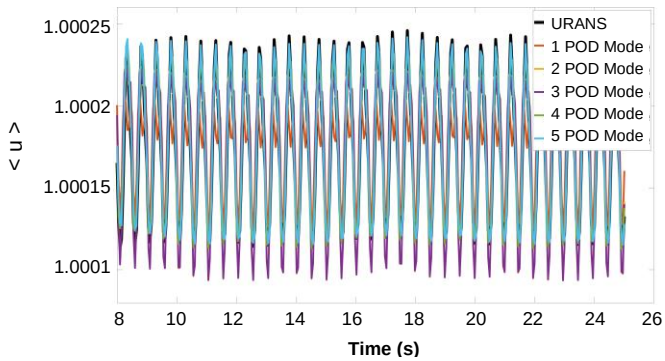

Fig. 7. Comparison of the reconstructed flow field with POD

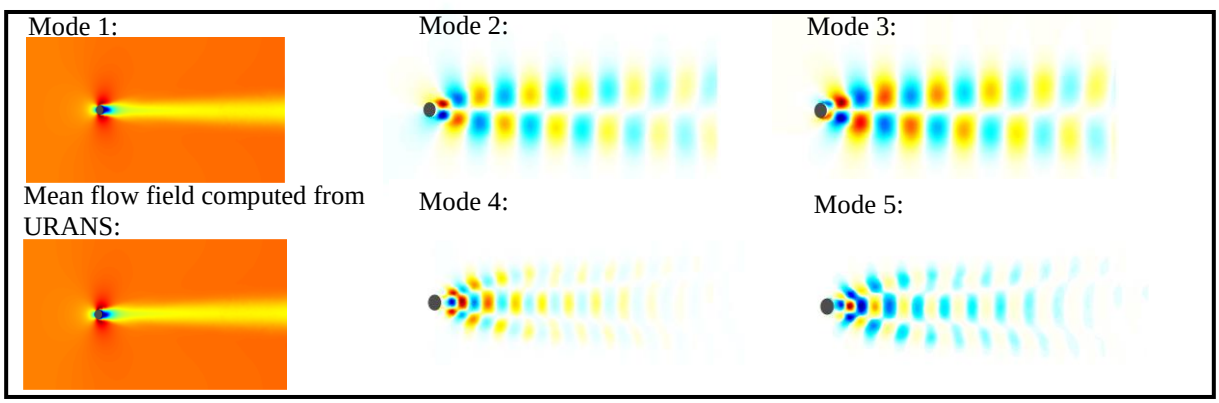

Fig. 8. The first five dominant POD modes.

4.3 Dynamic Mode Decomposition (DMD)

The 340 eigenvalues distribution in Fig. 9 demonstrates that every eigenvalue is in the unit circle, indicating that all DMD modes are stable. In Fig. 10, there are three modes that have significantly greater amplitude than the other DMD modes on the complex pairs. The second DMD mode is located at the frequency of 2.027 Hz, which is closed to the vortex shedding frequency. Figure 11 describes the flow field reconstruction of the streamwise velocity. Similar to POD, as the number of DMD modes employed for the flow reconstruction increase, the streamwise velocity of the reconstructed flow field becomes closer to the original streamwise velocity obtained from URANS. The first three modes present the spatial structures in both real and complex parts (Fig. 12). It is likely that the first DMD mode represents the mean flow field at the frequency of 0 Hz. The second and third DMD modes demonstrate extracted structures, which resemble POD and there are connected to mechanisms of vortex shedding. The free shear layer on both sides has rolled up in the mechanism for the second DMD. The interaction between the vortex and vortex is seen

in the third DMD mode. The additional information that obtained from DMD is the DMD mode which decay in time. This mode was found at the frequency 2.39 Hz, which is the ninth DMD mode. The ninth mode's spatial structures in both real and imagination are shown the vortices cut off state for beginning to shed, which is the procedure of vortex shedding mechanisms. As seen in Fig. 13, the orange vortex on the lower side essentially cut off the blue free shear layer at the top.

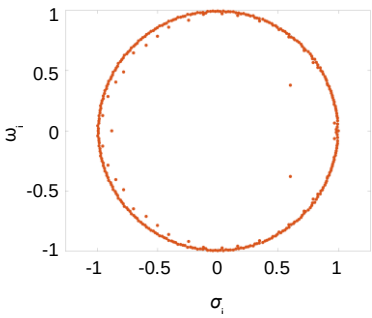

Fig. 9. Eigenvalues distribution.

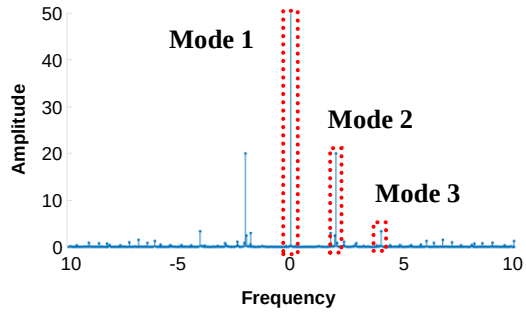

Fig. 10. DMD amplitude distribution vs frequencies.

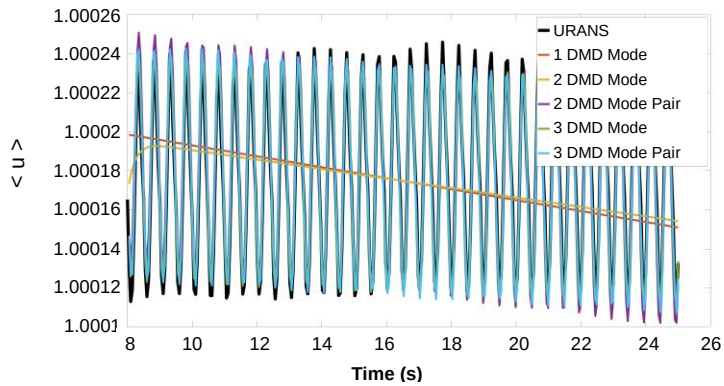

Fig. 11. Comparison of the distribution vs frequencies reconstructed flow field with DMD.

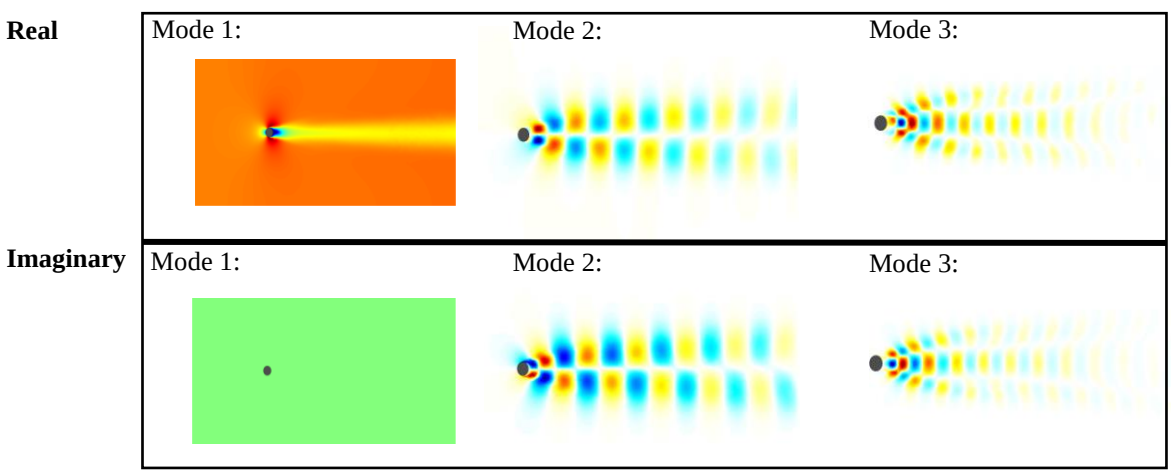

Fig. 12. The first three dominant DMD modes with complex conjugate pairs.
Mode 1 (f = 0 Hz); Mode 2 (f = 2.027 Hz); Mode 3 (f = 4.054 Hz).

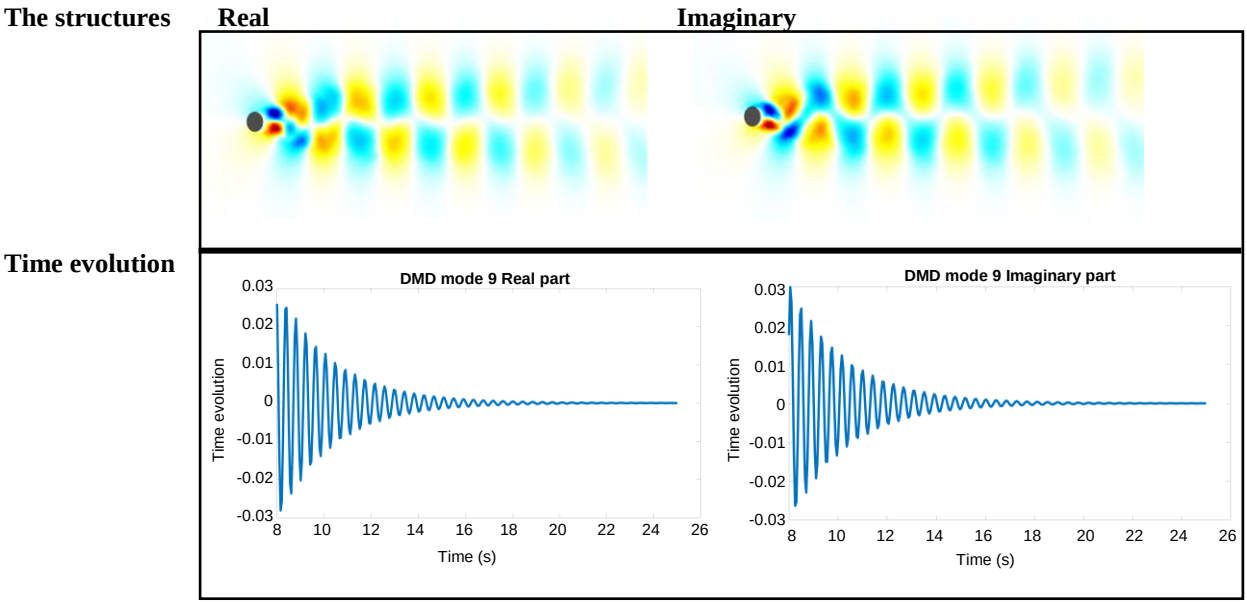

Fig. 13. The spatial structure both real and imaginary part at DMD mode 9 (f = 2.39 Hz).

4.4 Spectral Proper Orthogonal Decomposition (SPOD)

Figure 14 presents the first energy mode of the 17 frequencies, which obtained from applying 340 snapshots to SPOD. Clearly, there are three distinct frequencies at 1.25 Hz, 1.875 Hz and 2.5 Hz, which contain greater mode energy than others. The highest mode energy is at the frequency of 1.875, which is closed to the vortex shedding frequency. The spatial structure of the SPOD modes at these three distinct frequencies reveals the large-scale structures with alternating pattern, which are in state of rolled-up free shear layers that related to the vortex shedding mechanisms as shown in Fig. 15. These three modes exhibit disturbance with no decay in time. While the decay modes are not detected.

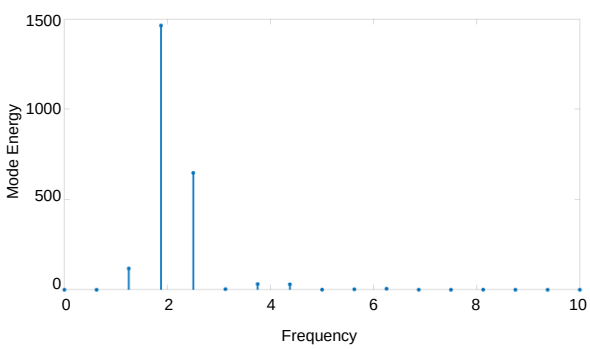

Fig. 14. SPOD mode energy of each 17 frequencies

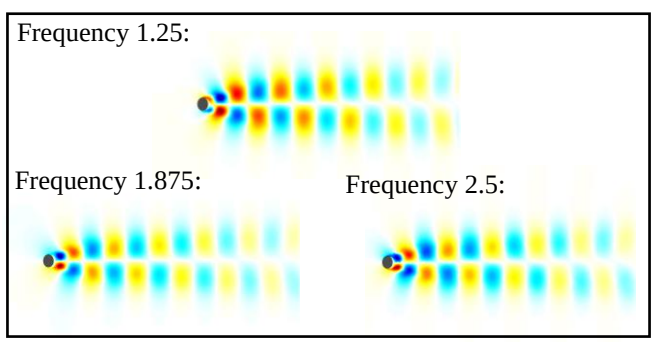

Fig. 15. Spatial structure of SPOD mode energy (f =1.25, 1.875, and 2.5 *Hz*)

5. Conclusion

Spectral analysis of flow around a circular cylinder at a subcritical Reynolds number is explored and compared via POD, DMD, and SPOD. From POD and DMD, it demonstrates that the spatial structures representing the most dominant mode is the mean flow field. On the other hand, SPOD excludes the mean flow field from the analysis. The large-scale spatial structures of POD mode 2 and 3 are similar to the ones derived from the DMD second mode pair, illustrating the free shear layers rolled up state of vortex shedding mechanisms at specific frequencies. The symmetrically alternating structures are presented along the top and bottom sides of the cylinder's centerline. Moreover, smaller scales of vortex street-like structures obtained from POD mode 4 and 5 are similar to the one

extracted from the DMD third mode pair. It is suggested that these additional small scaled structures behind the cylinder are the influence of vortex-vortex interactions between the top and bottom sides before they diffuse and decay into three shedding lines. It is the mechanism of eddy shedding in high-speed mode. Physics may imply that the free shear layers rolled up state and the influence of the vortex's interaction are effect along the flow without degradation due to the no decay in time evolution. Contrary to the vortices cut off the free shear layer state, which the decay in time. It demonstrates that this state temporarily affects the flow.

The three data-driven method have different pros and cons. The capability of POD to reconstruct the flow field using fewer modes is demonstrated. However, DMD and SPOD are able to extract significant modes associated with distinct frequencies. The frequencies of 2.027 and 1.875 Hz, close to the vortex shedding frequency of 1.96 Hz, were detected via DMD and SPOD, respectively. DMD can offers variety of frequencies. As a result, the ninth DMD mode, which decays in time can be identified. On the other hand, because of its noisy spectrum, it's hard to analyse. While in SPOD the decay mode cannot detected. The explanation is because SPOD, which based on Welch's method for averaging spectrum techniques, it's reduced the spectral precision and only detected significant modes. Thus, the number of snapshots must be increased in order to obtain greater precision in the spectrum using the default parameters. SPOD provides the energy rank associated with the mode energy in each frequency from high to low. The pattern of SPOD frequency spectra which removes the mean flow from the analysis is similar to the pattern derived from the spectral analysis of C_L values. When the frequency is closed to the vortex shedding frequency, the mode energy increases and reaches its peak at the vortex shedding frequency before being damped in subsequent frequencies. While in POD and DMD is interrupted by the static mode.

The underlying physics of flow around a circular cylinder at a subcritical Reynolds number is derived from POD, DMD and SPOD analysis. The extracted modes will be used to create a reduced-order model (ROM) of flow past a circular cylinder. Then, active flow control of the vortex-shedding flow will be able to develop based on ROM.

Acknowledgement

We would like to thank and delight those who supported this research and we are very grateful to the Department of Mechanical Engineering, Faculty of Engineering, King Mongkut's University of Technology Thonburi for computing facilities.

Nomenclature

$\bar{u}$	mean velocity, m/s
$\bar{p}$	mean pressure, Pa
ν	kinematic viscosity, m^2/s
τ	Reynold stress, N/m^2
ρ	fluid density, kg/m^3
μ_t	dynamic eddy viscosity, Pa s
ψ, U	POD modes
$\sum$	Rectangular diagonal matrix
Φ^T, V^T	transpose of complex unitary matrix
ϕ	DMD modes
W	weight matrix
$\tilde{\psi}$	SPOD modes
C_D	drag coefficient
C_L	lift coefficient
Re	Reynolds number

References

[1] Douglas JF, Gasiorek JM, Swaffield JA, Jack LB. Fluid mechanics. 5th ed. Harlow: Pearson education; 2005.
[2] Stringer RM, Zang J, Hillis AJ. Unsteady RANS computations of flow around a circular cylinder for a wide range of Reynolds numbers. Ocean Eng. 2014;87:1-9.

[3] Menter FR. Two-equation eddy-viscosity turbulence models for engineering applications. AIAA J. 1994;32(8):1598-1605.
[4] Norberg C. Effects of Reynolds number and a low-intensity freestream turbulence on the flow around a circular cylinder. Publikation. 1987;87(2):1-55.
[5] Holmes P, Lumley JL, Berkooz G, Rowley CW. Turbulence, coherent structures,dynamical systems and symmetry. Cambridge: Cambridge University Press; 2012.
[6] Schmid PJ. Dynamic mode decomposition of numerical and experimental data. J Fluid Mech. 2010;656:5-28.
[7] Taira K, Brunton SL, Dawson STM, Rowley CW, Colonius T, McKeon BJ, et al. Modal analysis of fluid flows: An overview. AIAA J. 2017;55(12):4013-4041.
[8] Lienhard JH. Synopsis of lift, drag, and vortex frequency data for rigid circular cylinders (Vol. 300). Pullman: Technical Extension Service; 1966.
[9] Sieber M, Paschereit CO, Oberleithner K. Spectral proper orthogonal decomposition. J Fluid Mech. 2016;792:798-828.
[10] Liu H. Large eddy simulation of flow past a 3D cylinder at Re= 3900. IOP Conf Ser: Mater Sci Eng. 2018;383(1):012050.
[11] Rajani BN, Kandasamy A, Majumdar S. LES of flow past circular cylinder at Re= 3900. J Appl Fluid Mech. 2016;9(3):1421-1435.